IC/90/166

INTERNATIONAL CENTRE FOR
THEORETICAL PHYSICS

THE ROTATION OF ACCRETION-DISKS AND THE POWER SPECTRA OF X-RAY "FLICKERING"

Xiao-He Zhang

and

Gang Bao

INTERNATIONAL
ATOMIC ENERGY
AGENCY

UNITED NATIONS
EDUCATIONAL,
SCIENTIFIC
AND CULTURAL
ORGANIZATION

1990 MIRAMARE - TRIESTE

IC/90/166

International Atomic Energy Agency
and
United Nations Educational Scientific and Cultural Organization
INTERNATIONAL CENTRE FOR THEORETICAL PHYSICS

THE ROTATION OF ACCRETION-DISKS AND THE POWER SPECTRA OF X-RAY "FLICKERING" *

Xiao-He Zhang
International Centre for Theoretical Physics, Trieste, Italy

and

Gang Bao
Scuola Internazionale Superiore di Studi Avanzati, Trieste, Italy.

MIRAMARE – TRIESTE
July 1990

ABSTRACT. The X-ray producing, inner region of the accretion disk in Active Galactic Nuclei (AGN) is likely to be non-stationary and non-axisymmetric. This non-stationarity and non-axisymmetry in disk surface brightness may be modeled by considering the presense of many "hot spots" on a steady, axisymmetric disk. As long as a "spot" can survive for a few orbital periods, its orbital frequency can be introduced into the light curve either by relativistic orbital motion or by eclipsing of the spot by the disk. These rotational effects vary with the local properties of the spot population. Depending on the radial variation of spot brightness, lifetime and number density, the observed variability power spectrum may differ from that due to the intrinsic variability of spots alone, within the orbital frequency range in which these spots occur. In this paper, we explore the relation between properties assumed for the spot population and the resulting predictions for the observered variability. The implications of our results for the "flickering" of X-ray sources powered by accretion disks (both AGN and galactic sources) are also discussed.

* Submitted for publication.

I. Introduction

It is well known that the inner portion of an accretion disk suffers thermal and viscous instabilities (Shakura and Sunyaev, 1976, Lightman and Eardley, 1974, Lightman, 1974, Pringle *et. el.*, 1973). The perturbations will grow fast enough to destroy the stationary, axisymmetric state which one generally assumes, although they will subsequently saturate to give a stable state, as a result of nonlinear effects and under the constraint of a relatively constant accretion rate at the outer edge of the disk. Under typical conditions, the inner part of an AGN accretion disk will resemble a collection of lumps, orbiting around the central black hole, rather than a smooth, axisymmetric plate or a doughnut (if it is a thick disk). A particular numerical example of a disk being broken into "planets" can be found in the paper by Hawley (1987). Because of the huge local shear of the orbital motion (which always exists), any relatively large lumps produced by instabilities will be smeared out very quickly or may even be prevented from growing to a large scale, and only small ones can exist for a relatively long time. However, even the latter will still be destroyed at larger thermal timescales (Pringle, 1981). Apart from the density variations, we may also have other types of non-axisymmetric variations, like the magnetic flares, shocks or convective cells, in this part of the accretion disk. Due to the otherwise lack of theoretical modeling of temporal and spatial evolution of the inner regions of accretion disks, it seems reasonable to adopt a phenomenological approach at this stage. Instead of introducing another model for this non-stationary, non-axisymmetric fluctuation in the disk surface brightness, we will approximate this non-axial symmetry and non-stationarity, which may come from a variety of particular models, by a distribution of lumps (or "hot spots" to be more descriptive) spread randomly on the surface of the disk, with certain prescribed distribution functions for their lifetime τ, brightness I_0 and their surface number density n, all varying with the radius. When these spots orbit the central compact object at relativistic speeds, the intensity of X-ray radiation arriving at the detector will change periodically with the orbital period of the spots, either due to Doppler effect (Sunyaev, 1973) or because of the eclipsing of photons from these spots by either the outer edge of the disk or the funnel wall. As a result, the observed X-ray intensity will have components changing at the orbital frequencies of all of the spots present. The envelope of the overlapping power

spectrum profiles due to the individual spots will give us a broad feature in the observed power spectrum. Since the orbital period is generally shorter than the timescales in various models describing the intrinsic variability of AGN's, the rotation-induced change described above can be important for systems not observed face-on. Thus although the behavior of the spots themselves is very important in understanding the short term time variability of X-ray intensities ("flickering") of AGN and of galactic X-ray sources (Lehto, 1990, Begelman, 1990), the orbital motion should also be included in studying the variability. It is the purpose of this paper to study how the periodic changes in light propagation (Doppler beaming, time delay, disk eclipsing) due to the orbital motion can convert the intrinsic variability into that actually observed.

The instabilities work most efficiently in the inner parts of the disk and the disk is smoother as one moves out radially. This gives a cut-off frequency at the lower end where the lumpiness of the disk surface becomes small. The inner edge of the disk introduces a cut-off at the high frequency end. The variability would be affected by the rotation of the disk, and the brightness and the number density of the spots on the disk surface between these two cut-offs, but not so strongly outside this frequency range. Therefore we would expect the power spectra of the variability to take different forms as these two frequencies are crossed if the rotation is to play any role at all. For galactic sources, they appear to be the "knee" frequency at the lower end and features near the QPO (quasi-periodic oscillation) frequency at the higher end (Makishima, 1988). For AGN's the data is not sufficiently good and complete yet to give any strong indication about either cut-off and we probably still observe the variability between these two cut-off frequencies.

In this paper, we will concentrate on how the orbital motion of the spots can change the observed variability for various given properties of spot population. For simplicity and also to focus on the main points of this paper, we neglect the general relativistic corrections to the photon trajectories, i.e., we do not consider gravitational deflection of the X-ray photons. This will restrict our results to being more appropriate for accreting systems having a neutron star as the central compact object. However, even for Schwarzschild black holes, as long as the disk is not viewed very close to edge-on, the general relativistic corrections will not change our results significantly (Sec. 2). We will also assume that

matter along the light path is relatively optically thin for the X-ray photons in the energy range of interest. For optically opaque media, different absorption for photons emitted at different spot positions would give another source of rotation-induced variability. How this could enhance the effect discussed in this paper will be explored in the future but is not considered here. Since the variability of BL Lac objects is generally believed to be associated with material ejected from the central part, the results presented here do not seem to apply to that class of objects.

The basic idea on which this paper is based is described in Abramowicz *et. el.* (1990). A brief outline of the derivation of our equation (3.14) is also given there. Here we give a more general derivation and discuss in more detail the assumptions made and the potential implications of the results. More numerical examples are also given here. In Sec. 2, we first derive the expression for the time variation of intensity due to one single spot having a relativistic orbital speed, and then in Sec. 3, we derive the general expression [Eq. (3.10)] of power spectra for light curves with contributions from many spots. Using this general expression, we discuss what we would expect under the most simplified and ideal condition and give an expression for the variability power spectrum in the power-law form [Eq. (3.14)] to illustrate the relative importance of various spot properties. In Sec. 4, we show our numerically simulated light curves and the corresponding power spectra. The potential relation between these results and present and future observational data is also discussed towards the end of the paper. Some details of the derivations are presented in several appendices.

II. Rotational effect due to one "hot spot"

The light curves generated by a finite sized star, orbiting in the equatorial plane around an arbitrary black hole, have been computed by Cunningham and Bardeen (1973), using a hybrid numerical and graphical method (see also Asaoka, 1989 for a more recent, purely numerical approach). In this paper, we will not consider the general relativistic effects on the light trajectories. This enables much of the calculation of a light curve to be done analytically.

It is well known (see, e.g., Misner, Thorne and Wheeler, 1973) that along the null geodesics,

$$I_\nu/\nu^3 = \text{constant}. \tag{2.1}$$

The total intensity of a light source, integrated over its effective frequency range, is changed by a factor of the fourth power of the redshift factor, g,

$$I_{obs} = g^4 I_{em} \quad . \tag{2.2}$$

The redshift factor is, by definition, the ratio of the observed energy of a photon, E_{obs}, to the energy of the photon in the rest frame of the source, E_{em},

$$g \equiv E_{obs}/E_{em} \quad . \tag{2.3}$$

For a distant observer moving at non-relativistic speed, we can approximate the four-velocity of the observer as

$$\vec{u}_{obs} = (1,0,0,0) \quad . \tag{2.4}$$

Here and in the following, we use spherical coordinates and the geometric units in which $G = c = 1$.[1] The observed photon energy, in term of the four-momentum $\vec{P}$ of the photon, is

$$E_{obs} = -\vec{u}_{obs} \cdot \vec{P} = -P_t \quad . \tag{2.5}$$

However, the light source, i.e., the spot, is carried by the accretion disk in orbital motion in the gravitational field of the central object. The four-velocity of the spot is

$$\vec{u}_s = \frac{1}{\sqrt{1-2M/r_s - v_{orb}^2}}(1,0,0,\Omega_s) \quad , \tag{2.6}$$

with

$$v_{orb} \equiv \Omega_s r_s \sin\theta_s \quad . \tag{2.7}$$

Here M is the mass of the central object, Ω_s is the orbital frequency and the spot orbit is indicated by (r_s, θ_s). The energy of a photon emitted in the rest frame of spot is therefore,

$$E_{em} = -\vec{u}_s \cdot \vec{P} = -\frac{P_t + \Omega_s P_\phi}{\sqrt{1-2M/r_s - v_{orb}^2}} \quad . \tag{2.8}$$

[1] In this unit, $10^7 M_\odot = 49\text{sec} = 1.5 \times 10^{12}\text{cm}$.

By decomposing $\vec{P}$ in the local inertial frame of the spot, one can readily find P_ϕ (see Appendix A) and consequently the redshift factor,

$$g = \frac{\sqrt{1-2M/r_s}}{\sqrt{1-2M/r_s - v_{orb}^2}}(\sqrt{1-2M/r_s} - v_{orb}\sin i \sin\phi_s) \quad . \tag{2.9}$$

Here i is the inclination angle of the orbital plane (Fig. 1).

In general, to convert the orbital position of the spot ϕ_s to the photon arrival time t at the detector, one needs to integrate the differential equations of the photon trajectory (Cunningham and Bardeen, 1973), and to find t as a function of, say, r along a specific trajectory. Fortunately, it is trivial to integrate these equations in flat spacetime: all light rays follow straight lines and the light travel time is simply the distance traveled by the photon divided by the speed of light. However, one needs to be careful in that the light travel time is different for photons emitted from different orbital positions, unless the disk is seen face-on. This difference in travel time, as compared with photons that would be emitted at the center of the orbit, can also be calculated very easily (see Fig. 1),

$$\Delta t = -\frac{v_{orb}}{\Omega_s}\sin i \cos\phi_s \quad . \tag{2.10}$$

Therefore, as a function of the arrival time, the intensity of light from a spot changes periodically,

$$I_{obs} = \left(\sqrt{\frac{1-2M/r_s}{1-2M/r_s - v_{orb}^2}}(\sqrt{1-2M/r_s} - v_{orb}\sin i \sin\phi_s)\right)^4 I_{em}. \tag{2.11}$$

Here

$$\phi_s = \Omega_s t + \phi_0 + v_{orb}\sin i(\cos\phi_0 - \cos\phi_s) \quad . \tag{2.12}$$

We have chosen $t = 0$ to be the moment at which the first photon emitted from the spot after its creation arrived at the detector, and ϕ_0 to be the orbital position at which the spot was created. Note that if $\Delta t = 0$ then the highest harmonic in I_{obs} would be $4\Omega_s$, but the nonlinearity of (2.12) in ϕ_s introduces all high harmonics into I_{obs}. These high harmonics, $n\Omega_s$ die out of course as $(v_{obs}\sin i)^n$. Since the flux is simply the product of the intensity and the solid angle subtended by the spot at the observer, the flux changes

in the same way as the intensity if the general relativistic effect on the photon trajectories is not included. The error introduced by this is discussed at the end of this section.

The expression derived above is for the orbits which are not partially eclipsed. The eclipsing will occur when, for example, the spot orbit is located deep in the funnel wall of a thick disk, or the inclination angle is quite large and the disk is flaring (see Fig. 2). When there is eclipsing of the spot, the intensity at the observer is found from (2.11) and (2.12), plus the condition

$$I_{obs} = 0 \ , \qquad |\phi| \le \phi_{eclipse} \tag{2.13}$$

Before we study the collective behavior of many spots, we would like first to estimate how large the error in (2.12) could be when the general relativistic effects on light trajectories are neglected. We shall have the same type of error when we use (2.11) to compute the observed flux, treating the solid angle subtended by the spot as a constant. The error is of order

$$M/b$$

where b is the impact parameter of photon trajectory. This could significantly alter our result if b is very close to M, a probable situation when the disk is seen close to edge-on. In this case the light-rays will graze the horizon of the black hole. We would no longer be able to approximate light trajectories as straight lines, and consequently to treat the solid angle subtended by the spot at the observer as an orbital-position independent quantity or to compute Δt in the way described above. This, of course, will not happen with a system in which a neutron star (of radius r_*) is the central object, since M/b can never be larger than

$$M/r_* \lesssim 0.1 \quad .$$

For AGN's, the inner region is more likely to be blown up by the radiation pressure. If we restrict attention to moderate inclination angles and consider the spots to be on the surface of a moderately thick disk, then ignoring the deflection of photons will not introduce serious errors into (2.12). One can estimate (Appendix B) that in terms of the emission angle i_0 and the spot position r_0, θ_0 (see Fig. 3), the deflection angle is roughly,

$$|\Delta i_\infty| \simeq \frac{(i_0+\theta_0)^3 M}{r_0} \quad , \tag{2.14}$$

for $\theta_0 \lesssim i_0$. For

$$i_0 = \theta_0 \lesssim 1/4 \simeq 15^\circ,$$

we would have

$$|\Delta i_\infty| \lesssim (1/2)^3 \frac{M}{r_0} \simeq \frac{M}{8r_0} \quad ,$$

which is not a very large correction.

To conclude, Eqs. (2.11), (2.12) describe the intensity variation to a reasonably good approximation for spots orbiting a non-rotating compact object, even for black hole systems having moderate inclination angle of the orbital plane.

III Time variation due to many "hot spots" and its power spectrum

As have been discussed in Introduction, we shall approximate the innermost, X-ray producing region of the accretion disk as consisting of two components: that due to a steady and axially symmetric "disk" component, L_D, and the contribution from all of the spots, L_S,

$$L = L_D + L_S. \tag{3.1}$$

The time and angle averaged L could be computed from a disk model. The spots are assumed to have average values as functions of the radius for their brightness, $I_0(r)$, lifetime, $\tau(r)$ and the number of spots per unit interval of radius, $n(r)$. The explicit functional forms for these quantities should be given by some specific model describing the intrinsic variability. Because when $\tau(r)$ is longer than a few orbital periods, observations cannot easily differentiate different intrinsic variabilities with the same $I_0(r)$, $\tau(r)$ and $n(r)$, we will not discuss any particular intrinsic variability here. In the following, we derive a general expression for the observed power spectrum [Eq. (3.10)] for any given intrinsic variability, with the rotational effect included.

The power spectrum of a time sequence $I(t)$ is defined (see, for example, Bendat and Piersol, 1971) as

$$P(\omega) = \lim_{\Delta\omega\to 0} \frac{< I^2(t,\omega,\Delta\omega) >}{\Delta\omega} \quad . \tag{3.2}$$

This measures the strength of the signal $I(t)$ at frequency ω. In the following, we shall first compute the power spectrum for the time variability [Eqs. (2.11–13)] produced by orbiting spots, i.e., due to L_S. From this general expression, we will then discuss how the statistics and rotation of the spots can alter the observed variability of light curves.

Using the Wiener-Khintchine theorem, the power spectrum of $I(t)$ is related to its auto-correlation function $R(t_0)$ through

$$P(\omega) = \int R(t_0) e^{-i\omega t_0} dt_0 \quad . \tag{3.3}$$

From the definition of $R(t_0)$,

$$R(t_0) \equiv \lim_{T\to\infty} \frac{1}{T} \int_{t_1}^{t_1+T} I(t) I(t+t_0) dt_0 \quad , \tag{3.4}$$

(here t_1 is arbitrary for stationary processes) we can then write the power spectrum of $I(t)$ in terms of its Fourier transform $S(\omega)$,

$$P(\omega) = \frac{1}{2} \lim_{T\to\infty} \frac{1}{T} |S(\omega)|^2 \quad . \tag{3.5}$$

The signal $I(t)$ is contributed to by many spots during the observation time T. We must add the contributions from all of these spots,

$$P(\omega) = \frac{1}{2} \lim_{T\to\infty} \frac{1}{T} \sum_i |S(\omega; r_i, \phi_i, t_i)|^2 \quad . \tag{3.6}$$

Here $S(\omega; r_i, \phi_i, t_i)$ is the Fourier transform of $I_i(t)$ for the i^{th} spot created at the location (r_i, ϕ_i) and the time t_i. The summation is over all spots appearing during time T. If we treat the spot creation process to be stationary, consider spots created at the same radius to be identical, and factor out the constant part, I_0, of the redshifted intensity from $S(\omega; r_i, \phi_i, t_i)$; and if we convert the summation into an integral by introducing the probability function $n(r, \phi_0)$ for a spot to be created at radius r and azimuthal angle ϕ_0,

normalized to the average number of spots on the surface of the disk, then we can also write

$$P(\omega) = \frac{1}{2}\int \frac{I_0^2(r)}{\tau(r)}|s(\omega, r, \phi_0)|^2 n(r, \phi_0) dr d\phi_0 \quad . \tag{3.7}$$

Here we define

$$I_0(r) \equiv \left(\frac{1 - 2M/r}{1 - 2M/r - v_{orb}^2}\right)^2 I_{em} \ , \tag{3.8}$$

and

$$s \equiv S/I_0 \ . \tag{3.9}$$

It is straightforward, though tedious, to show (Appendix C) that for axisymmetric $n(r, \phi_0)$,

$$n(r, \phi_0) = \frac{1}{2\pi} n(r) \ ,$$

and a (possibly eclipsing) neutron star or Schwarzschild black hole system,

$$\begin{aligned} P(\omega) &= \frac{1}{2}\int \frac{I_0^2(r)}{\tau(r)} n(r) p(r;\omega) dr \\ &= \frac{1}{2}\int \frac{I_0^2(r)}{\tau(r)} n(r) dr \sum \alpha_N (v_{orb}\sin i)^M J_N(K v_{orb}\sin i) G_{\omega - N_1\Omega} G^*_{\omega + N_2\Omega} . \end{aligned} \tag{3.10}$$

In order to write (3.10) in a compact form, we have used a few abbreviations. The full expressions are given in Appendix C. More specifically, K, M, N, N_1, N_2 are merely symbolic representations of some integers; α_N corresponds to the N^{th} numerical expansion coefficient; $J_N(x)$ is the N^{th} order Bessel function; G_ω is the Fourier transform of the evolution function $G(t)$ due to the intrinsic variability in the spot's own rest frame, and G^*_ω denotes its complex conjugate. The situations where $N = 0$ but $N_1, N_2 \neq 0$ will occur only when there is an eclipse. It is also to be noted that $M + N$ is always an even number, which can be understood from the time reversal symmetry of the disk motion.

From this general expression, we can see that, as one would expect, the resulting power spectrum is controlled by the rotation law $\Omega(r)$ of the disk and the radial dependences of the spot number density $n(r)$, the spot brightness $I_0(r)$ and the spot lifetime $\tau(r)$. In particular, for a ring of spots not observed face-on ($\sin i \neq 0$), in addition to the intrinsic variability (G_ω), one can also see the rotation-induced variability ($G_{\omega - n\Omega}$). The strength of the repeated feature depends on the $2n^{th}$ power of the projected orbital speed of the

spots on the ring, $(v_{orb}\sin i)^{2n}$, and the total intensity of all of these spots. When the spots are spread in a large range of radii, the rotation will introduce a broad feature into the power spectrum in the frequency range of the corresponding orbital frequencies.

To study further the effects of rotation and statistics of spots on the observed variability, let us consider a simple case where

$$G(t;\tau) = \begin{cases} 1 & t_0 < t < t_0 + \tau(r) \\ 0 , & \text{otherwise} \end{cases} ; \tag{3.11}$$

and treat the disk as being geometrically thin so that no eclipse needs to be considered. We will also ignore the relativistic corrections to the orbital motion. Since typically, even for a Schwarzschild black hole,

$$(v_{orb}\sin i)^2 = (\Omega r \sin i)^2 \ll 1 \quad ,$$

this will not be a serious limitation even for black hole systems. Then as long as

$$\frac{1}{\tau} \ll \Omega$$

we can approximate G_ω as

$$G_\omega \sim \frac{\sin\frac{(\omega - \Omega)\tau}{2}}{(\omega - \Omega)}$$

and the summation in (3.10) will be dominated by the first non-trivial terms (we are not interested in the $\omega = 0$ component here). Therefore, we have

$$\begin{aligned} P(\omega) &\sim \int \frac{I_0^2(r) n(r) (\Omega r \sin i)^2}{\tau} \left(\frac{\sin\frac{(\omega - \Omega)\tau}{2}}{(\omega - \Omega)}\right)^2 dr \\ &\sim \left[I_0^2(r) n(r) (\Omega r \sin i)^2 \tau(r) \left(\frac{dr}{d\Omega}\right)\right]\Bigg|_{\Omega = \omega} . \end{aligned} \tag{3.12}$$

From this, we readily see that if $I_0(r), n(r)$, and $\tau(r)$ follow power-laws as functions of r,

$$I_0(r) \sim r^{-\alpha_I} \quad , \quad n(r) \sim r^{1-\alpha_n} \quad , \quad \tau(r) \sim r^{\alpha_\tau} \quad , \tag{3.13a}$$

and if the disk rotation can also be described in power-law form,

$$\Omega(r) \sim r^{-\alpha_\Omega} \quad , \tag{3.13b}$$

then the resulting power spectrum $P(\omega)$ will also have a power-law form,

$$P(\omega) \sim \omega^{1+\frac{2\alpha_I+\alpha_n-\alpha_r-4}{\alpha_\Omega}} \sin^2 i \quad . \tag{3.14}$$

One interesting consequence of (3.14) is that, for uniform radial distribution of the statistical properties of the spots ($\alpha_n = \alpha_r = \alpha_I = 0$) and for a Keplerian disk ($\alpha_\Omega = 3/2$), the power spectrum has the form

$$P(\omega) \sim \omega^{-5/3} \sin^2 i \quad . \tag{3.15}$$

It should be mentioned that while the simple power-law form (3.14) tells us roughly how the variability changes with the statistical properties of the spots and the rotation of the disk, it is obtained when eclipsing and the Lorentz factor of the orbital speed are omitted. If we put back the Lorentz factor, (3.14) will no longer be in exactly a power-law form. It will then tend to be less steep near to the highest orbital frequency because the actual contribution from spots of larger orbital frequency is larger than when the Lorentz factor is ignored. It should also be noted that while (3.15) gives a definite number, $-5/3$, for the power-law index, it is obtained for an overly simplified and, perhaps, unrealistic spot population. In general, one tends to have fewer spots away from the inner edge of the disk ($\alpha_n \gtrsim 0$), and this is likely to introduce a flattening of the power spectrum at the low frequency end. One would also expect that the variation in disk surface brightness is weaker and slower at larger distances ($\alpha_I \gtrsim 0$, $\alpha_r \gtrsim 0$), which would further flatten the power spectrum at the low frequency end. Concerning the rotation law, the disk is expected to be intermediate between a Keplerian disk ($\alpha_\Omega = 3/2$) and a constant specific angular momentum torus ($\alpha_\Omega = 2$). It should also be pointed out here that if the spots are caused completely by viscous processes and the total radiation from the spots is strictly proportional to that in the underlying steady, axisymmetric disk, then one would have $\alpha_I + \alpha_n \lesssim 3$ (Shakura and Sunyaev, 1973). To have a negative logarithmic slope in the power spectrum, as has been observed, one would need $\alpha_I \lesssim 1$ and $\alpha_n \gtrsim 2$. Thus it seems that a viscous disk would have to put unproportionally more energy into spots at larger radii in order to reproduce the observed power spectrum and it is tempting to exclude viscosity as being primarily responsible for the spot production. However, because of the

lack of detailed studies of non-axisymmetric and non-stationary accretion disks, it is still largely unknown which values α_I, α_r and α_n will take. Some careful analysis of the time evolution of non-axisymmetric disks seems to be needed in order to give one any reasonable estimate for these statistical properties of the spots. At the end of this paper, we will give some further discussion of the properties of spots in terms of their relation to the observable features.

IV. Numerical Simulations and Discussion

To show better the effect of rotation and of the statistical properties of spots on the observed variability as given by (3.10), and to avoid the limitations due to the assumptions on spot motion leading to (3.14), we have also made some simple numerical simulations of light curves and have estimated the power spectra directly from these simulated light curves. We approximate the disk to be geometrically thin so that all of the spots are orbiting the central object in the equatorial plane. To generate these light curves, we first assign each spot a randomly selected creation time t_i. We then assign the initial positions r_i of these spots randomly according to their average lifetime $\tau(r)$ and the average number of spots per unit interval of radius $n(r)$. The initial angular position ϕ_i is assigned randomly and uniformly within the interval $0 \leq \phi_i < 2\pi$. The resulting light curve at time t is found by summing the fluxes from all of the contributing spots and the contribution from each spot is computed using Eqs. (2.11), (2.12). The number of spots on the disk surface at any given time is estimated from the observed amplitude of the variability. Using $\Delta I_s/I_s \sim 2$ for a spot at $r = 10M$ [Eq. (2.11)], taking $\Delta I/I \sim 10\%$ as a canonical number from the observations and assuming that $L_S/L_D = 1/3$, we estimate that, from the statistics of spot, an average of 100 spots on the disk surface is consistent with observations. This is the number which we use in the simulations. To simulate any possible instrumental noise or noise inherent to the signal, L_D also contains a 10% noise contribution. The innermost orbit ($r_{in} = 10M$) is divided into 32 zones and 4000 orbits are taken between r_{in} and r_{out}. The outermost orbit considered is at $r_{out} = 80M$. Each orbit is divided uniformly, with each zone corresponding to approximately the same duration for all these orbits.

In Fig. 4 we first show the simplest case, with $G(t)$ taking the form (3.11). The lifetime τ is the same for all of the spots and is chosen to be 4 times the orbital period of the outermost orbit. The spots are distributed uniformly on the surface of the disk and have equal brightness. In Fig. 4a the disk is viewed face-on and no variability can be seen apart from that due to the switching on and off of the spots and that of the noise. In Figs. 4b, c, d, the effect of rotation gradually appears as the inclination angle i is increased: that part of power spectrum due to spot rotation increases above the noise level and its shape changes until it reaches the power-law form, $P(\omega) \sim \omega^{-1.5}$. Here the slight departure of β from that predicted by (3.15) is basically due to the larger Lorentz factor and larger variation in time delay at the smaller radii (i.e., at larger orbital frequencies). Note that, once it has risen above the noise level and dominates the intrinsic part, the changed slope of the power spectrum is completely determined by the disk rotation and the statistical properties of the spots; while the inclination angle mainly controls the amplitude.

In Fig. 5, we use an $n(r)$ with a decrease in the surface number density of spots beyond $r \approx 30M$ in order to model the tendency of the disk to be smoother at larger radii. All of the other parameters are the same as in Fig. 4. The inclination angle is $i = 60°$. This simulation was made in order to demonstrate that the spatial distribution of spots will make a difference to the apparent variability when the disk is seen with a non-zero inclination angle. In particular, when there is a drop in the spot density beyond a certain radius, the power spectrum could be flattened below the corresponding orbital frequency.

Finally, to demonstrate that the observed variability can be different from the intrinsic variability, we give $G(t)$ the form of an exponential decay,

$$G(t) = \begin{cases} e^{-(t-t_i)/t_0}, & t > t_i; \\ 0 & \text{otherwise} \end{cases} . \qquad (4.1)$$

Here the e-folding time t_0 is 4 times the orbital period of the innermost orbit ($\Omega(r_{in})t_0 = 8\pi$). Therefore we would expect that the power spectrum be different near the highest orbital frequency but change little below $\omega \lesssim 2\pi/t_0$. The rotation law is $\Omega \sim r^{-2}$ and is normalized so that the innermost orbit will have the same orbital frequency as a Keplerian one. Because of the shorter effective lifetime of spots in this case and the limitation of computer capability, instead of keeping the effective average number of spots on the disk

surface the same, we here take $L_S/L_D = 50$. The range of radii is chosen to be from $r_{in} = 6M$ to $r_{out} = 50M$. It should be noted that the expression (2.11) does not quite apply for thin disks near to this r_{in}. The strong light bending and the consequent time delay will introduce a larger amplitude into the rotation-induced variability at the orbital frequency than that described by (2.11). In a subsequent paper, these two important effects for thin disks around a black hole or for large inclination angles will be included in a fully relativistic treatment. Nevertheless, we here use (2.11) to compute the simulated light curve and demonstrate that, just because of relativistic orbital motion, the observed variability (Fig. 6b) will be different from the intrinsic variability (Fig. 6a), when the timescale of the intrinsic variability is that of a few orbital periods. Since in general the orbital period is the smallest timescale, the orbital motion, as we repeat and emphasize here, is likely to change the apparent variability unless the variability is due to some global changes and the variation is axisymmetric.

Before concluding this paper, we would like to comment briefly on the potential connections between the results presented here and observations. It is found that for almost all of the sources, the power spectra of AGN X-ray light curves has a power-law form, $P(\omega) \sim \omega^{-\beta}$. The same is true for galactic black hole candidates and low-mass-X-ray-binaries (LMXB's) (See, for example, the review papers by Pounds and McHardy, 1988, McHardy, 1989, Makishima, 1988 and in the proceedings edited by Treves, 1987; but see also Mittaz and Branduardi-Raymont, 1989 and Fiore *et. al.*, 1989 for two possible exceptions.). This power-law behavior generally occurs in the range from hours to days for AGN's and 0.1Hz - 10Hz for galactic sources, a range which scales roughly with the central mass. Since these objects are all believed to be powered by the accretion and the disk motion must be relativistic for these systems, this similarity in the variability might just be related to the presence of "hot spots" on the surface of the disk. It should be pointed out that for AGN's the power-law indices β are scattered over a larger range (Table 1 in McHardy, 1989) between 1 and 2, while for LMXB's β varies slightly around 1.5 for different samples (Makishima, 1988). This is probably because the central objects of AGN's are more likely to be rotating black holes (Rees, 1984) and so the radius of the inner edge of the disk can be comparable with the gravitational radius. The uncertainty of the resulting

enhancement of the rotationally-induced variation for black hole systems may cause this larger variation in β.

As is clearly demonstrated by Fig. 5, if rotation is one of the important factors, any radial variation in spot properties will introduce certain observable structures into the variability power spectrum. The most noteworthy are the flattening of power spectra at the low frequency end, corresponding to the decrease of spot number and spot intensity at larger radii as first suggested by Shakura and Sunyaev (1976) and Nolan *et. el.* (1981); and the cut-off in power spectra at the high frequency end, corresponding to the absence of spots beyond the inner edge of the disk. The low frequency flattening could also be due to the exponential decay in time of spot intensity, but the high frequency cut-off seems to be more naturally associated with the absence of spots. There are a few clear-cut cases of low frequency flattening of the power spectra both for AGN's (e.g., Fig. 3 in McHardy, 1989 for NGC 5506) and for galactic sources (e.g., Fig. 2 in Nolan *et. el.*, 1981 and Fig. 3 in Makishima, 1988 for Cyg X-1). The situation at the high frequency end is generally less clear due to the high noise level there, with possibly the exception of Cyg X-1 for which an ensamble-averaged power spectrum in the X-ray energy band $1-24$ kev was obtained (Fig. 3 in Makishima, 1988). We can read off the cut-off frequency to be approximately 100Hz from this figure. This would correspond to a central mass in the range $14M_\odot \lesssim M \lesssim 60M_\odot$ if we take $8M \gtrsim r_{in} \gtrsim 3M$, to take into account the sharp decrease of radiation from disks very close to the innner edge of accretion disks and the effect on the radius of inner edge by the rotation of the central black hole. This estimate is not very different than the current observational estimate of $M = 16 \pm 5M_\odot$ (Gies and Bolton, 1986), though we may still need to look at higher energy band so that the reprocessing of signal by the intervening medium can be considered not important. Nevertheless, if the noise inherent in the signal (e.g., that due to flicker noise, which will always be present, or due to variations in the intervening medium) is not very high, then by reducing the instrumental error one might be able to observe features near to the cut-off and relate them to the central mass.

From the fact that the intrinsic variability timescales are generally longer than the local orbital period, we have been able to partially understand the X-ray variability power

spectrum. However, our present lack of knowledge about the spot production and destruction processes prevented us from making any fit of a particular model to the observational data, aside from pointing out the possible causes of some observed structures in the power spectrum. Some further study of non-stationary, non-axisymmetric accretion disks is clearly needed in order to understand the rich variability data now available and to extract useful information on the central engine from this data.

Acknowledgement

We would like to thank Marek Abramowicz for directing our attention to this problem, for numerous useful discussions and for his continuous interest and support. Some helpful discussions with Antonio Lanza are also gratefully acknowledged. We also thank John Miller for a careful reading of the manuscript. One of the authors (X.H.Z.) would like to thank Professor Abdus Salam, the International Atomic Energy Agency and UNESCO for hospitality at the International Centre for Theoretical Physics, Trieste.

Appendix A

For a spot orbiting the central object at angular frequency Ω_s and orbital speed v_{orb}, the four velocity is

$$\vec{u}_s = \frac{1}{\sqrt{1-2M/r_s - v_{orb}^2}}(1,0,0,\Omega_s) \quad . \tag{A1}$$

We choose the comoving orthonormal basis to satisfy

$$\vec{e}^{(i)} \cdot \vec{e}^{(j)} = \delta_{ij} \quad i,j = r,\theta,\phi; \tag{A2a}$$

$$\vec{e}^{(t)} \cdot \vec{e}^{(\mu)} = -\delta_{t\mu} \ , \quad \mu = t,r,\theta,\phi \ . \tag{A2b}$$

In component form, they are

$$\vec{e}^{(t)} = \vec{u}_s = \frac{1}{\sqrt{1-2M/r_s - v_{orb}^2}}\left(\frac{\partial}{\partial t} + \Omega_s \frac{\partial}{\partial \phi}\right) , \tag{A3a}$$

$$\vec{e}^{(r)} = \sqrt{1-2M/r_s}\frac{\partial}{\partial r} \ , \quad \vec{e}^{(\theta)} = \frac{1}{r_s}\frac{\partial}{\partial \theta} \ , \tag{A3b}$$

$$\vec{e}^{(\phi)} = \frac{1}{\sqrt{1-2M/r_s - v_{orb}^2}}\left(\frac{v_{orb}}{\sqrt{1-2M/r_s}}\frac{\partial}{\partial t} + \frac{\sqrt{1-2M/r_s}}{r_s \sin\theta_s}\frac{\partial}{\partial \phi}\right) \ . \tag{A3c}$$

Then, using the definition of P_ϕ, we find

$$\begin{aligned} P_\phi &\equiv \vec{P} \cdot \frac{\partial}{\partial \phi} \\ &= \frac{r_s \sin\theta_s}{\sqrt{1-2M/r_s - v_{orb}^2}} \vec{P} \cdot \left(\sqrt{1-2M/r_s}\vec{e}^{(\phi)} - v_{orb}\vec{e}^{(t)}\right) \\ &= \frac{\sqrt{1-2M/r_s}\ r_s \sin\theta_s}{\sqrt{1-2M/r_s - v_{orb}^2}}\left(\frac{v_{orb}}{\sqrt{1-2M/r_s}} - \sin i \sin\phi_s\right) E_{em} \quad . \end{aligned} \tag{A4}$$

Here i is the inclination angle of the orbital plane (see Fig. 1 in Sect. 2).

Appendix B

In the Schwarzschild geometry, the metric line element can be written as

$$ds^2 = -(1-2M/r)dr^2 + \frac{dr^2}{(1-2M/r)} + r^2(d\theta^2 + \sin^2\theta d\phi^2) \tag{B1}$$

By using two constants of motion,

$$P_t = -(1-2M/r)\frac{dt}{d\tau} \tag{B2}$$

and

$$P_\phi = r^2 \frac{d\phi}{d\tau} \quad , \tag{B3}$$

we can find the differential equation for photon trajectories by setting

$$ds^2 = 0 \ .$$

After some simplifications (see, for example, Misner, Thorne and Wheeler, 1973),[2] this can be written as

$$\left(\frac{dx}{d\phi}\right)^2 = \frac{1}{b^2} - x^2 + 2x^3 \quad , \tag{B4}$$

where

$$b \equiv -\frac{P_\phi}{MP_t} \tag{B5}$$

is the dimensionless impact parameter of the photon trajectory and

$$x \equiv \frac{M}{r} \tag{B6}$$

is the dimensionless Schwarzschild radial coordinate along it. The deflection angle for a photon emitted at x_0 is

$$\Delta\phi_\infty \equiv |\phi_\infty - \phi_0| = \int_{x_0}^{0}\left(\frac{b_{Sch}}{\sqrt{1-b_{Sch}^2x^2+2b_{Sch}^2x^3}} - \frac{b_F}{\sqrt{1-b_F^2x^2}}\right)dx \tag{B7}$$

where one requires that

$$\frac{1}{b_{Sch}^2} + 2x_0^3 = \frac{1}{b_F^2} \ ,$$

so that the photon emission angle is the same in both the Schwarzschild and flat spacetimes. For photon trajectories far from the horizon and having no turning point ($dx/d\phi = 0$), we have

$$\Delta\phi_\infty \approx b^3 x_0^4 \quad . \tag{B8}$$

[2] In this appendix, the equatorial plane, $\theta = 90°$, is the photon trajectory plane, and ϕ_0, ϕ_∞ differ from i_0 and i_∞ of Sect. 2 by θ_0.

For moderate emission angles ($\phi_0 \lesssim 1$), we can make the approximation $bx_0 \approx \phi_0$ and then

$$\Delta\phi_\infty \approx x_0\phi_0^3 \quad . \tag{B9}$$

Appendix C

In this appendix, we will use the definition

$$v_p \equiv v_{orb}\sin i$$

for the projected orbital speed of a spot. The light curve of a spot can be represented as

$$u(t) = (1 - v_p\sin\phi_s)^4 E(\phi_s)G(t) \tag{C1}$$

where I_0 has been factored out [Eq. (3.8)] and

$$\phi_s = \Omega_s t + \phi_0 + v_p(\cos\phi_0 - \cos\phi_s) \quad . \tag{C2}$$

Here, we use $E(\phi_s)$ to represent the eclipse,

$$E(\phi_s) = \begin{cases} 1 & |\phi_s - 2n\pi| > \phi_{\rm eclipse}, n = 0, \pm 1, 2, \ldots \\ 0 & \text{otherwise} \ ; \end{cases} \tag{C3}$$

$G(t)$ is the evolution envelope of the spot intensity due to the intrinsic variability; and we assume that the spot has an equal probability of being produced at any orbital position ϕ_0.

In terms of the Fourier transforms of $u(t)$, we can write down the power spectrum for $u(t)$ due to a spot at radius r,

$$p(r;\omega) = \frac{1}{4\pi}\int_0^{2\pi} d\phi_0 \int_{-\infty}^{+\infty} dt \int_{-\infty}^{+\infty} dt' \times \\ \times (1 - v_p\sin\phi_s)^4(1 - v_p\sin\phi_s')^4 E(\phi_s)E(\phi_s')G(t)G(t')e^{-i\omega(t-t')} \ . \tag{C4}$$

To evaluate (C4), we first make a Fourier series expansion of $E(\phi_s)$,

$$E(\phi_s) = \sum_n b_n e^{in\phi_s} \quad . \tag{C5}$$

We also write, for the sake of compactness,

$$(1 - v_p\sin\phi_s)^4 = \sum_{k=0}^{4}\binom{4}{k}(-v_p)^k\sin^k\phi_s \quad , \tag{C6}$$

$$\sin^k\phi_s = \left(\frac{1}{2i}\right)^k (e^{i\phi_s} - e^{-i\phi_s})^k \\ = \frac{e^{ik\phi_s}}{(2i)^k}\sum_{j=0}^{k}\binom{k}{j}(-1)^j e^{-i2j\phi_s} \quad . \tag{C7}$$

The orbital position ϕ_s may be solved from (C2) by an iterative method,

$$\phi_s^{(0)} = \Omega_s t + \phi_0 \quad ,$$

$$\phi_s^{(1)} = \phi_s^{(0)} + v_p(\cos\phi_0 - \cos\phi_s^{(0)}) \quad ,$$

$$\phi_s^{(2)} = \phi_s^{(0)} + v_p(\cos\phi_0 - \cos\phi_s^{(1)}) \quad ,$$

$$\ldots$$

and stopping at the first step. The truncation error for $u(t)$ is

$$\frac{\Delta u}{u} = \frac{4v_p|\sin\phi_s - \sin\phi_s^{(1)}|}{|1 - v_p\sin\phi_s|} \\ = \frac{8v_p|\cos\frac{\phi_s+\phi_s^{(1)}}{2}\sin(\frac{v_p(\cos\phi_s - \cos\phi_s^{(1)})}{2})|}{|1 - v_p\sin\phi_s|} \\ = \frac{8v_p|\cos\frac{\phi_s+\phi_s^{(1)}}{2}\sin\left(v_p\sin\frac{\phi_s+\phi_s^{(1)}}{2}\sin(\frac{v_p(\cos\phi_s - \cos\phi_s^{(1)})}{2})\right)|}{|1 - v_p\sin\phi_s|} \\ = \ldots \tag{C8}$$

It is clear that this error approaches zero more quickly than any power of v_p for small v_p, which is the case for both neutron star and Schwarzschild black hole systems. For $\phi_s \approx \phi_s^{(1)}$, we make a further expansion,

$$e^{-i(n+k-2j)v_p\cos(\Omega_s t+\phi_0)} = \sum_{p=0}^{\infty}\sum_{s=0}^{P}\frac{1}{(2p)!!}\binom{p}{s}[-i(n+k-2j)v_p]^p e^{i(p-2s)(\Omega_s t+\phi_0)} \ . \tag{C9}$$

Similar expansions are made for $(1 - v_p \sin\phi_s')^4$ and $E(\phi_s')$ with the following changes in indices,

$$n \to n' \ , \quad k \to m \ , \quad l \to j \ , \quad p \to q \ , \quad r \to s \ . \qquad (C10)$$

Of the three integrals in (C4), we integrate first over ϕ_0 with the aid of the integral representation of the n^{th} order Bessel function

$$J_n(x) = \frac{1}{2\pi i^n} \int_0^{2\pi} e^{ix\cos\phi - in\phi} d\phi$$

and the final result is

$$p(r;\omega) = \sum \alpha_N (v_p)^M J_N(K v_p) G_{\omega - N_1\Omega_s} G^*_{\omega + N_2\Omega_s} \qquad (C11)$$

Here one should expand the abbreviations $\sum$, α_N, N, M, K, N_1, N_2 as follows:

$$\sum \to \sum_{\substack{k=0 \\ m=0}}^{4} \sum_{j=0}^{k} \sum_{l=0}^{m} \sum_{\substack{n=-\infty \\ n'=-\infty}}^{\infty} \sum_{\substack{p=0 \\ q=0}}^{\infty} \sum_{s=0}^{p} \sum_{r=0}^{q} \qquad (C12)$$

$$\alpha_N \to \binom{4}{k}\binom{k}{j}\binom{4}{m}\binom{m}{l}\binom{p}{s}\binom{q}{r} b_n b_{n'} \frac{(n+k-2j)^p (n'+m-2l)^q (-1)^{p+q+s+r}}{2^{k+m+p+q} p!\, q!\, i^{n+n'}} \qquad (C13)$$

$$N_1 \equiv 2j - k - p + 2s - n \ , \quad N_2 \equiv 2l - m - q + 2r - n' \ , \quad N = N_1 + N_2 \ , \qquad (C14)$$

$$K \equiv k + m + n + n' - 2(j+l) \ , \quad M \equiv k + m + p + q \ . \qquad (C15)$$

Correct to order v_p^3, Eq. (C11) becomes

$$\begin{aligned} p(r;\omega) = {} & 3(3 + 4v_p^2) \frac{\sin^2 \frac{\omega\tau}{2}}{(\omega)^2} \\ & + 4v_p^2 \left[\frac{\sin^2 \frac{(\omega-\Omega_s)\tau}{2}}{(\omega-\Omega_s)^2} + \frac{\sin^2 \frac{(\omega+\Omega_s)\tau}{2}}{(\omega+\Omega_s)^2} \right. \\ & \left. - \left(\cos\frac{\Omega_s\tau}{2}\right) \frac{\sin\frac{\omega\tau}{2} \sin\frac{(\omega-\Omega_s)\tau}{2}}{\omega(\omega-\Omega_s)} - \left(\cos\frac{\Omega_s\tau}{2}\right) \frac{\sin\frac{\omega\tau}{2} \sin\frac{(\omega+\Omega_s)\tau}{2}}{\omega(\omega+\Omega_s)} \right] \\ & + O(v_p^4) \quad . \end{aligned} \qquad (C16)$$

References

1. Abramowicz, M., Bao, G., Lanza, A., and Zhang, X.-H., 1990, submitted to *Astrophys. J. Lett.*
2. Asaoka, I., 1989, *Publ. Astron. Soc. Japan*, **41**, 763
3. Begelman, M., 1990, in *Variability of Active Galactic Nuclei*, eds. H. R. Miller and P. J. Wiita
4. Bendat, J. S., Piersol, A. G.: 1971, *Random Data*, John Wiley & Sons, Chap. 1
5. Cunningham, C. T., and Bardeen J. M.: 1973, *Astrophys. J.* **183**, 237-264
6. Fiore, F., Massaro, E., Perola, G.C., and Piro, L.: 1989, *Astrophys. J* **347**, 171
7. Gies, D. R., and Bolton, C. T.: 1986, *Astrophys. J* **304**, 371
8. Hawley, J.: 1987, *Monthly Notices Roy. Astron. Soc.* **225**, 677
9. Lehto, H., 1990, in *Variability of Active Galactic Nuclei*, eds. H. R. Miller and P. J. Wiita
10. Lightman, A. P.: 1974, *Astrophys. J.* **194**, 419-427, and 429-437
11. Lightman, A. P., and Eardley, D. M.: 1974, *Astrophys. J.* **187**, L1 – L3
12. Makishima, K.: 1988, in *Physics of Neutron Stars and Black Holes* (ed. Y. Tanaka), Universal Academy Press, Tokyo, 175-189
13. McHardy, I.: 1989, in *Proceedings of the 23rd ESLAB Symposium* (ed. J. Hunt and B. Battrick), European Space Agency, The Netherlands, 1111-1124
14. Misner, C. W., Thorne, K. S. and Wheeler, J. A.: 1973, *Gravitation*, Freeman and Co., San Francisco
15. Mittaz, J. P. D., and Branduardi-Raymont, G.: 1989, *Mon. Not. R. A. Soc.* **238**, 1029–1046
16. Nolan, P. L., Gruber, D. E., Matteson, J. L., Peterson, L.E., Rothschild, R. E., Doty, J.P., Levine, A. M., Lewin, W. H. G., Primini, F. A.: 1981, *Astrophys. J.* **246**, 494–501

17. Pounds, K. A., and McHardy, I.: 1988, in *Physics of Neutron Stars and Black Holes* (ed. Y. Tanaka), 285-299 (Universal Academy Press, Tokyo)

18. Pringle, J. E.: 1981, *Ann. Rev. Astron. Astrophys.*, **19**, 137-162

19. Pringle, J. E., Rees, M. J., and Pacholczyk, A. G.: 1973, *Astron. Astrophys.* **29**, 179-184

20. Rees, M. J.: 1984, *Ann. Rev. Astron. Astrophys.*, **22**, 421-506

21. Shakura, N. I., and Sunyaev, R. A.: 1973, *Astron. Astrophys.* **24**, 337

22. Shakura, N. I., and Sunyaev, R. A.: 1976, *Mon. Not. Roy. Astron. Soc.* **175** 613-632

23. Sunyaev, R. A.: 1973, *Sov. Astron. AJ* **16**, 941-944

24. Treves, A., ed.: 1987, *Variability of Galactic and Extragalactic X-Ray Sources*, Associazione per l'Avanzamento dell'Astronomia, Milano-Bologna, 1-156

Figure Captions

Fig. 1 Illustration of a spot on the orbit (r_s, θ_s) at orbital position ϕ_s. The spatial legs of the orthonormal frame carried by the spot are $\{\vec{e}^{(r)}, \vec{e}^{(\theta)}, \vec{e}^{(\phi)}\}$. The orbital plane is inclined at an angle i, and the difference in travel time for a photon emitted at a particular orbital position (as compared with photons emitted at the orbital center) is Δt.

Fig. 2a When the orbit is deep in the funnel wall of a thick accretion disk, spots on the orbit could be eclipsed by the funnel wall.

Fig. 2b The flaring of a thin disk will also eclipse a spot when the inclination angle is high.

Fig. 3 The spot is on the orbit (r_0, θ_0). The initial emission angle of the photon is i_0, but due to gravitational deflection, the apparent angle measured by an observer at infinity is i_∞.

Fig. 4 Simulated light curves (top) and corresponding power spectra (bottom). These results are from calculations for 100 spots distributed uniformly between $10M$ and $80M$ on the surface of a Keplerian disk around a $10^7 M_\odot$ black hole. Once created, a spot is taken to survive for 4 times the orbital period of the outermost orbit, and to remain at a constant brightness during this time. The ratio between the luminosities in the disk and in the spot component is $L_S/L_D = 3$, with a 10% noise contribution to L_D. The inclination angle for Figure 4a (left) is 0°, for Figure 4b (right) is 20°.

Figure 4 (continue) Simulated light curves (top) and their power spectra (bottom) due to the same spot and disk configuration, but with increased inclination angle. For Figure 4c (left), the inclination angle is 40°; for Figure 4d (right), the inclination angle is 60°. Note that the logarithmic slope approaches -1.5 with increasing inclination angle.

Fig. 5 As the surface number density of spots drops beyond a certain radius, the power spectrum will be flattened below the corresponding orbital frequency. All parameters used here are the same as for Fig. 4, except that a different radial dependence of spot density is used. Figure 5a (top) shows the surface number density profile of the spots; Figure 5b (bottom) shows the variability power spectrum for an inclination angle $i = 60°$. Note the flattening of the power spectrum at low frequency and the the cut-off at the highest orbital frequency.

Fig. 6. The apparent variability can be different from the intrinsic variability because of the orbital motion of spots, if they can survive for a few orbital periods. In these diagrams, the intrinsic variability is described by an exponential decay, e^{-t/t_0}, and $\omega(r_{in})t_0 = 8\pi$. Fig. 6a (left): The simulated light curve (top) and the corresponding power spectrum (bottom) when the disk is seen face-on; Fig. 6b (right): The inclination angle here is 60°. Note the spot occured near the innermost orbit at time $t \approx 2 \times 10^5$sec in the portion of the light curve shown here. Note also the departure of the power spectrum from ω^{-2} for high orbital frequencies.

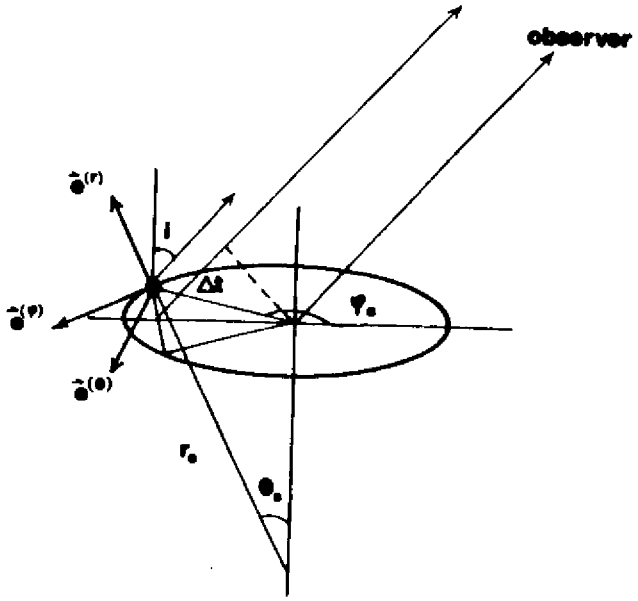

Fig.1

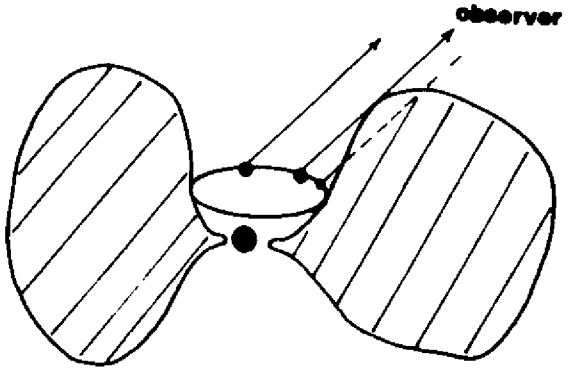

Fig.2a

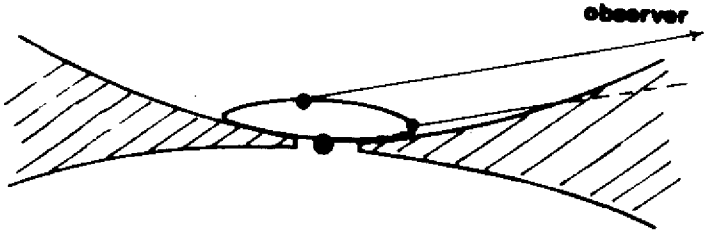

Fig.2b

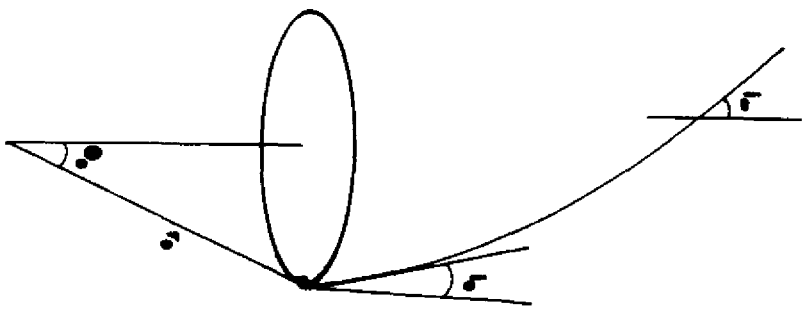

Fig.3

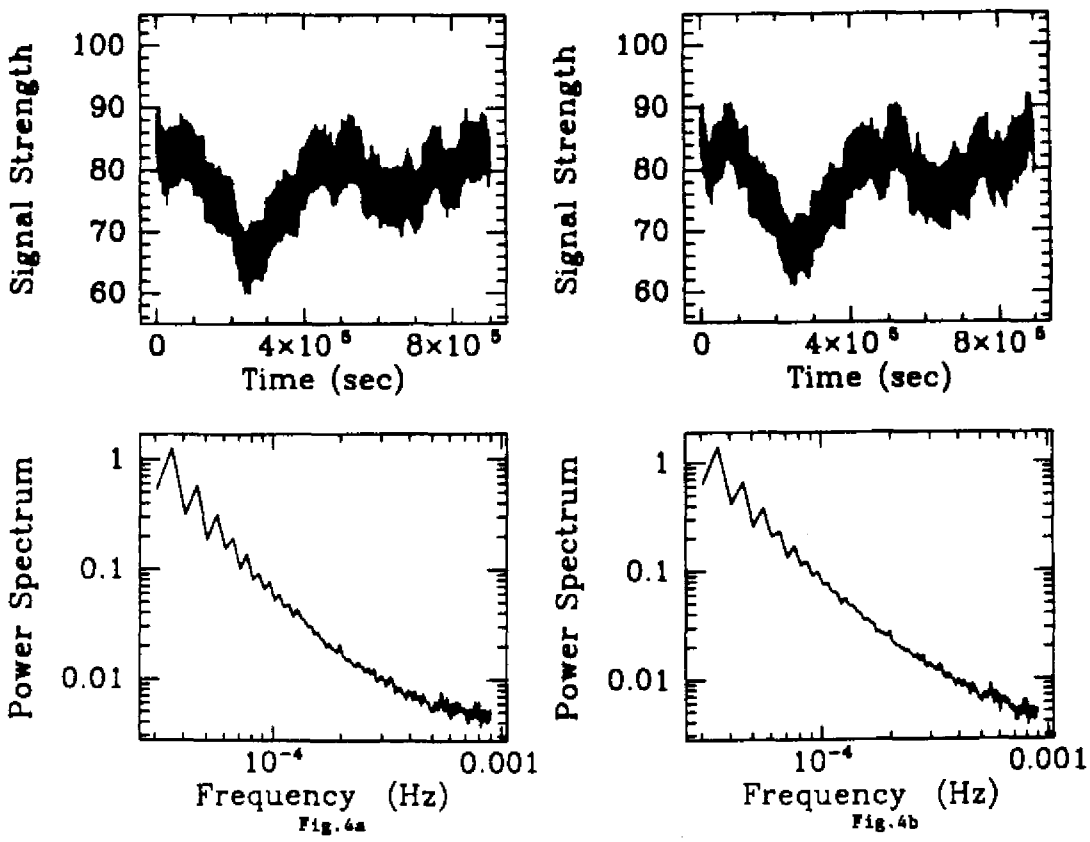

Fig.4a

Fig.4b

Fig.4c

Fig.4d

Fig.5

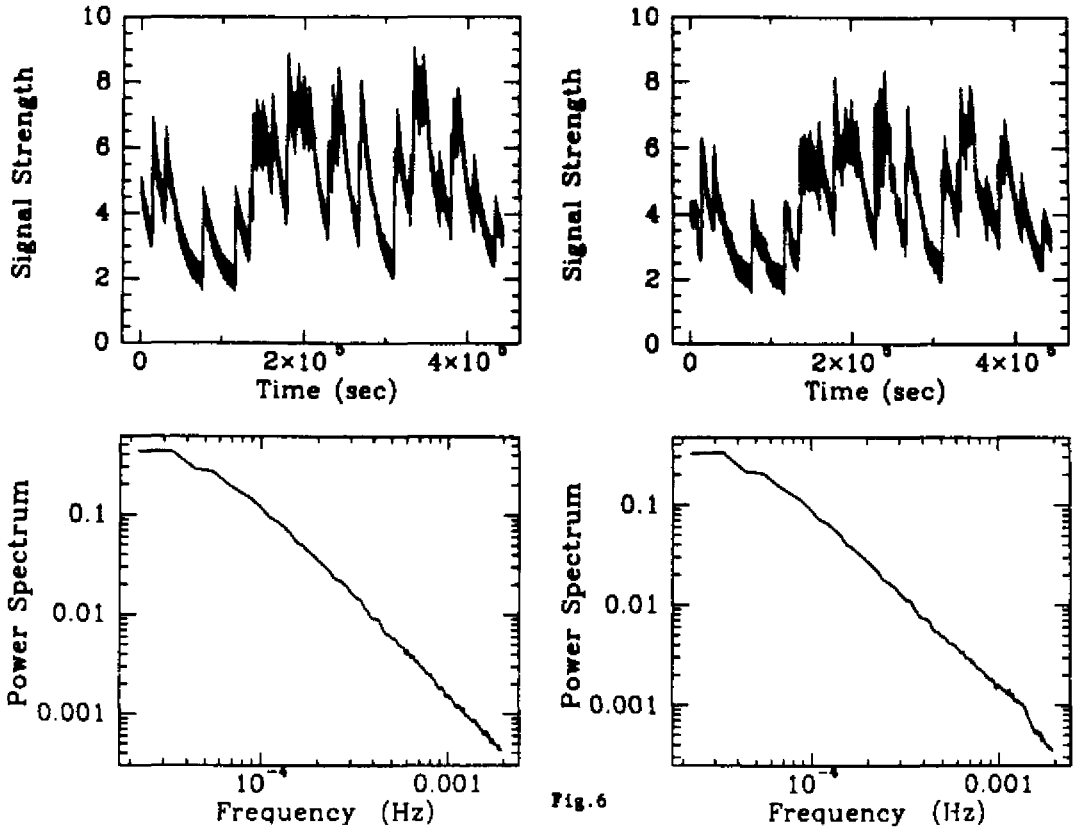
Signal Strength
10
8
6
4
2
0
0
2×10^5
4×10^5
Time (sec)
Power Spectrum
0.1
0.01
0.001
10^-4
0.001
Frequency (Hz)

Fig.6

Stampato in proprio nella tipografia
del Centro Internazionale di Fisica Teorica